

Oxygen/sulphur self-doped tunnel-like porous carbon from yellow bamboo for advanced supercapacitor applications

Erman Taer¹, Novi Yanti^{1,2}, Rahma Lia Putri¹, Apriwandi Apriwandi¹, Awaludin Martin³,
Julnaidi Julnaidi⁴, Nidya Chitranningrum⁵, Ahmad Fudholi^{6,7}, Rika Taslim^{2,8}

¹Department of Physics, Faculty of Mathematics and Natural Sciences, University of Riau, Riau, Indonesia

²Energy Research and Nano Carbon Center, Riau, Indonesia

³Department of Mechanical Engineering, Faculty of Engineering, University of Riau, Riau, Indonesia

⁴Department of Mechanical Engineering, Sekolah Tinggi Teknologi Pekanbaru, Riau, Indonesia

⁵Research Center for Biomass and Bioproduct, National Research and Innovation Agency, BRIN, South Tangerang, Indonesia

⁶Research Centre for Energy Conversion and Conservation, National Research and Innovation Agency, BRIN, South Tangerang, Indonesia

⁷Solar Energy Research Institute, Universiti Kebangsaan Malaysia, Bangi, Malaysia

⁸Department of Industrial Engineering, Faculty of Science and Technology, Universitas Islam Negeri Sultan Syarif Kasim Riau, Riau, Indonesia

Article Info

Article history:

Received Sep 13, 2024

Revised Apr 25, 2025

Accepted Jul 23, 2025

Keywords:

Chemical physical synthesis

Nanopores

Pores tunnels

Supercapacitor

Yellow bamboo

ABSTRACT

The 3D hierarchical pore structure with tunnel-like pores is essential to the performance of porous activated carbon (AC) materials used in symmetric supercapacitors. This study aimed to effect of adding (0.3, 0.5, and 0.7) M KOH reagent and heat treatment on the formation of 3D porous, tunnel-like AC derived from yellow bamboo (YB) through N₂-CO₂ pyrolysis at 850 °C. The AC produced had a high concentration of nanopores, becoming a valuable storage medium with favorable physical-electrochemical properties. The results showed that 0.5-YBAC had the best physical and electrochemical properties, with a carbon purity, 89.16%, micro crystallinity of 7.374 Å, and excellent amorphous porosity. Furthermore, 3D hierarchical pore structure, enriched naturally occurring heteroatoms, dopant of oxygen (10.14%) and sulfur (0.10%). A maximum surface area of 421.99 m² g⁻¹, along with a dominant combination of micro-mesopores. The electrochemical performance test of the 0.5-YBAC electrode showed a Csp of 214 F g⁻¹, with Esp 24.7 Wh kg⁻¹ and Psp 19.2 W kg⁻¹. In conclusion, this study showed the potential of YB stems to enhance the development of supercapacitors, offering superior porosity characteristics for efficient energy storage applications.

This is an open access article under the [CC BY-SA](#) license.



Corresponding Author:

Erman Taer

Department of Physics, Faculty of Mathematics and Natural Sciences, University of Riau

Simpang Baru, Riau 28293, Indonesia

Email: erman.taer@lecturer.unri.ac.id

1. INTRODUCTION

The threat of an impending electricity crisis is becoming more apparent. As electrical energy is fundamental to all human necessities and equipment, its availability poses several issues that significantly influence the environment, particularly through global warming. The issues have captured the attention of the community, prompting the advancement of science and technology to intensively focus more on developing solutions [1]-[3]. In response, the development of new and sustainable energy storage devices has become more important, driven by the pressing need for large-capacity electrical energy storage [4]. Rechargeable batteries and supercapacitors have developed as key forms of energy storage, attracting significant global study interest [5]. Although rechargeable batteries provide high-energy storage, they face challenges related to specific

power and cycle life, requiring further reviews to identify optimal solutions [6]. Conversely, supercapacitors offer significant advantages, including high specific power and long cycle life, making these devices well-suited for energy storage in electronic technology. The advancement of supercapacitors signifies substantial progress in energy storage technology [7]. Currently, numerous investigations are focusing on the potential of biomass, with its diverse natural characteristics, as a raw material for environmentally friendly and cost-effective supercapacitors. The performance of supercapacitors is also highly influenced by the types of materials used [8].

Biomass materials can generate nanoporous activated carbon (AC), which serves as an electrode material for supercapacitor cells due to its numerous benefits. These benefits include high porosity with varied morphology, a large specific surface area (SSA), excellent conductivity, thermal stability, and low production costs [9], [10]. Additionally, AC derived from biomass is believed to introduce natural heteroatoms into the carbon matrix. The heteroatoms in electrochemical test materials can trigger redox reactions, leading to pseudo-capacitance effects that enhance the electrochemical performance of supercapacitors. Consequently, this feature has become a focus in the study and development of supercapacitors, with the aim of enabling functional redox reactions in electrochemical processes [11]-[13]. The redox reactions can be facilitated by the availability of dopants such as oxygen (O), zinc (Zn), boron (B), sulfur (S), chlorine, and phosphorus (P), which are naturally occurring in biomass. Previous investigations, including those reported by Liu *et al.* [14], Jeloo *et al.* [15], and Zhang *et al.* [16], have documented the production of biomass-derived supercapacitors from garlic peels, barley straw, and coconut shell, indicating the use of nitrogen (N), O, and B heteroatoms doping. However, the dopants were sourced from external additives, resulting in more extended procedures, longer processing times, increased chemical use, and higher costs [17].

Selecting electrode materials that enhance the performance of supercapacitors as energy storage devices requires identifying optimal material characteristics through precise and accurate synthesis methods [18], [19]. In this study, bamboo was selected as a base material for supercapacitor electrode production due to its abundant availability and renewable nature [20], [21]. Additionally, the base material is widely distributed across tropical regions, with approximately 1500 species, making it a significant natural resource, particularly in Indonesia. Bamboo is traditionally used in the manufacture of furniture (chairs and tables) and as a fuel source. The flexibility and strength of the bamboo stem also make the material suitable for building construction [22]. With the modernization of technology and a growing demand for sustainable products, this base material is being developed for environmentally friendly technologies, such as renewable energy solutions. Bamboo stems can be carbonized at high temperatures to produce nanoporous carbon materials useful for energy storage devices, particularly supercapacitors [23]-[25]. However, AC derived from the stems has unique morphological structures, such as interconnected pores and high porosity. The high porosity is expected to achieve maximum C_{sp} values, making it a suitable raw electrode material [8], [26]. Previous investigations have reported that bamboo stems could be processed into supercapacitor electrodes using NaOH chemical treatment at varying concentrations [27]. The results showed that the optimal electrode condition was achieved with a 0.5 M activator concentration, resulting in a C_{sp} of 92 F g^{-1} . Yue *et al.* [25] and Jalalah *et al.* [28] reported that bamboo-based supercapacitor electrodes had C_{sp} of 236.35 F g^{-1} and 456 F g^{-1} , respectively, after being activated with CH_3COOK and KOH . These investigations used a conventional 3-electrode system to achieve superior electrochemical performance. They also adopted non-conductive materials that were detrimental to green synthesis and environmentally friendly supercapacitor technology. The use of chemical activators during the preparation of AC from biomass waste has a significant influence on the characteristics of the final carbon. Various chemical activators, including KOH , ZnCl , NaOH , and H_3PO_4 , significantly impact the properties of AC [23], [29]-[31].

This study investigates the impact of different KOH concentrations (0.3, 0.5, and 0.7 M) on the production of yellow bamboo activated carbon (YBAC) with high amorphous porosity and a 3D hierarchical pores structure suitable for efficient energy storage as well as improved supercapacitors performance, using a simple, non-template method that does not require additional chemical reagents. KOH was selected as the activating agent because it had the ability to increase the surface area of AC to generate more micro-mesopores [32]. Additionally, the chemical activator is considered to be cost-effective and readily available. YBAC was produced using a modified furnace equipped with smokeless and energy-efficient technology, which allowed for larger quantities and reduced processing time. The addition of KOH catalyst at an optimal concentration during chemical activation facilitated the formation of nanopores and supported the natural doping of O and S heteroatoms into the YBAC framework at appropriate levels. These factors contributed to the superior supercapacitor performance observed in 0.5-YBAC electrodes, which had a high C_{sp} of 214 F g^{-1} . The testing parameters were set within a potential window of 1-1000 mV, with a current density of 1 A g^{-1} in an aqueous $1 \text{ M H}_2\text{SO}_4$ electrolyte, using a symmetric 2-electrode solid system. The energy and power density obtained were 24.7 Wh kg^{-1} and 192 W kg^{-1} , respectively. Therefore, this study aims to examine the significant influence of pre-carbonization heat treatment in the furnace, varying low-scale KOH concentrations, and high-temperature $\text{N}_2\text{-CO}_2$ pre-activation combustion on the amorphous porosity, 3D hierarchical nanopores structure formation, chemical composition, and electrochemical performance of YBAC. The study becomes the 1st to

report the synthesis of YBAC waste using various KOH concentrations (0.3, 0.5, and 0.7 M) in order to produce AC as electrodes material for high-performance supercapacitors.

2. METHOD

2.1. Conversion of YB stem waste into AC

To ensure the quality of the samples, the condition of YB stems needed to be properly checked, with a focus on their physical appearance, size, and cleanliness. Dirty stem waste was washed using running water before being sliced into 5-10 cm pieces to speed up the drying process. A total of 5 kg of dry YB stem samples were converted into C using a modified furnace, a combustion method with heat distribution for 1 hour. The C produced was washed using distilled water with a soaking method for 1 week, with the water changed every day. To achieve a neutral pH and thorough cleaning, the C was dried in the sun for 3 days before being dried in a low-temperature oven at 110 °C for 2 days. The dried C particles were then crushed to a micro-scale with a mortar and ball milling tool for 1 day. Furthermore, the carbon powder was manually sieved to guarantee uniform particle size, using a 56 µm mesh size. The conversion of YB stem into AC began with the chemical activation treatment of KOH at different concentrations (0.3, 0.5, and 0.7 M). Initially, 30 g of carbon powder was mixed with KOH solutions of the requisite concentrations (2.52, 4.4, and 5.88 g), with the provision that the ratio of C and distilled water was 1:5. The mixture was homogenized on a hot plate with a magnetic stirrer at 80 °C and 300 rpm for 3 hours.

2.2. Physical and electrochemical characterization

The morphology of YBAC samples was observed using the field emission scanning electron microscope (SEM) method along with a Jeol JSM-IT200 equipment (No. BMN 3.08.03.07.001) after platinum spraying treatment. The analysis of X-ray diffraction (XRD) using a Rigaku SmartLab instrument with Cu K α radiation (36 kV, 30 mA) showed the amorphous-crystalline structure. The elemental composition test of the sample was carried out using energy dispersive spectroscopy (EDS) with a Hitachi SU-3500 instrument. The N₂ adsorption/desorption was tested through the use of a Mack ASAP2460 adsorbent meter at a temperature of 77 K. Furthermore, the SSA and pores size distribution of the material were calculated using the Brunauer-Emmett-Teller (BET) and the density functional theory (DFT) methods, respectively. The research scheme for converting yellow bamboo stems into activated carbon for supercapacitor electrode material is shown in Figure 1.

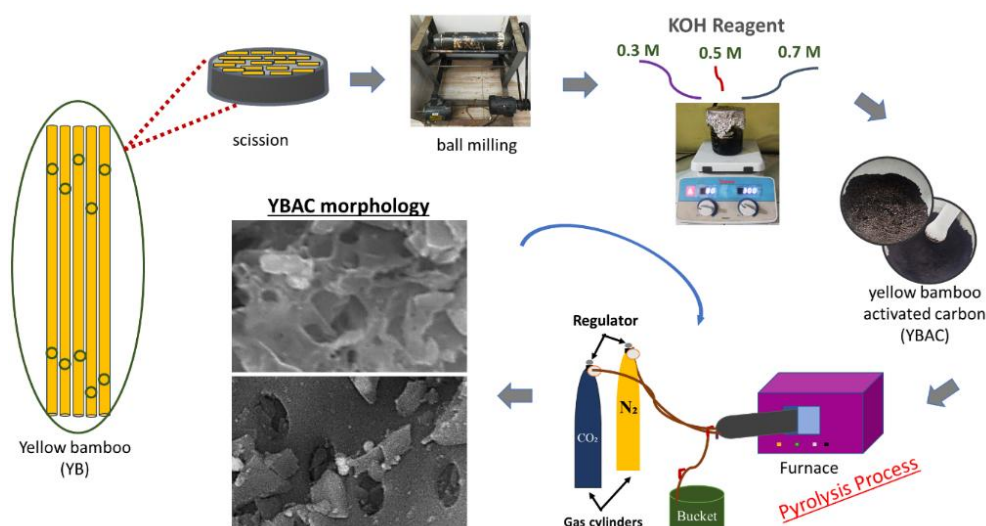


Figure 1. Research scheme for converting YB waste into YBAC as a basic material for supercapacitors

The characterization of electrochemical properties was tested using the cycle voltammetry (CV) and galvanostatic charge-discharge (GCD) methods. The test was conducted through the use of the physics CV UR Rad-ER 5481 and GCD UR Er 2018 instruments. Additionally, PVA adhesive was used to create symmetrical monolithic coin electrodes with a diameter of 7-8 mm and a thickness of 0.2-0.3 mm. Each electrode variant was immersed in 5 ml of 1M H₂SO₄ liquid electrolyte for 2 days to ensure that there was perfect absorption.

The test was carried out within a potential window of 0-1000 mV, with scan rate variations of (1, 2, and 5) mV s⁻¹ for the CV test as well as current density variations of 1, 2, and 5 A g⁻¹ for the GCD test.

3. RESULTS AND DISCUSSION

The microcrystalline structure of YBAC samples was validated by XRD, which assessed the degree of crystallinity and amorphous-crystalline nature, shown in Figure 2. In general, XRD pattern showed 2 sloping peaks and several sharp peaks in the 2θ scattering angle, within the range of 10-60°. The sloping peaks were correlated with the hkl 002 and 100 planes, signifying good amorphous and graphite-like carbon structures [33]. On the other hand, several sharp peaks were validated from the availability of non-carbon elements [34]. The data for XRD was processed using Microsoft Origin software to obtain the lattice parameter values. XRD pattern for 0.3-YBAC samples, with a lower activator concentration had higher intensity and less amorphous nature [35], [36]. The sloping peaks occurred at 22.08° and 44.02° (2θ), while a sharp peak at 36.26° was attributed to ZnO compounds (JCPDS No. 086-2339 and 047-1373), and another at 47.53° indicating the presence of CaCO₃ (JCPDS No. 82-1690). When the optimal KOH concentration treatment at 0.5-YBAC produced a more sloping diffraction pattern, there would be high amorphous porosity. Finer particle sizes and increased porosity caused a change in the diffraction angle to 22.96° and 43.69° (2θ), respectively. This analysis was supported by SEM measurements and N₂ gas absorption through the appearance of morphology and high surface area [37]. Furthermore, the activator treatment at 0.7-YBAC caused the X-ray intensity to further increase, reducing the amorphous nature of the sample. The presence of crystalline elements in YBAC samples was verified in small amounts, as evidenced by the EDS results in the following discussion. Table 1 presented the lattice parameters, including variations in 2θ due to the addition of KOH concentration. The d_{002} value of YBAC samples was greater than that of graphite (3.33 Å), suggesting a better amorphous structure. The height (L_c) and width (L_a) of the microcrystalline layer were inversely proportional to each other, with a small L_c value resulting in a larger SSA, which supported the high capacitance value of AC [38], [39].

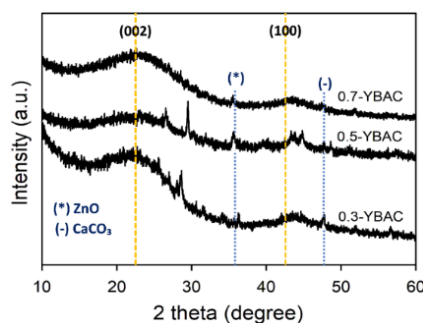


Figure 2. Patterns of the XRD curves for each variation of the YBAC sample

EDS analysis of YBAC samples found extensive information about the availability of chemical elements, as evidenced by intensity peaks at various energy levels. As detailed in Table 1, the results showed that natural elements such as C, O, S, potassium (K), Zn, sodium (Na), and silica (Si) were present in different percentages. These elements were obtained from the content of natural biomass materials and chemical-physical activation treatments through the use of KOH reagents, N₂, and CO₂ gas [40], [41]. YBAC samples were dominated by the presence of C elements, followed by lower amounts of other elements. For instance, the 0.3-YBAC sample comprised 82.94% C and 4.23% O, which acted as self-doping heteroatoms. A small percentage of K (0.2%) was found, originating from the addition of KOH reagents in the chemical activation process. The C content of the 0.5-YBAC sample increased to 89.16%, while natural O heteroatoms increased to 10.14%, and S was optimized at 0.10%. The addition of KOH reagent to the 0.7-YBAC sample resulted in an increase in C content of 89.89% but a decrease in O heteroatoms to 9.45%, as well as the loss of S. Furthermore, the availability of K increased to 0.31% due to the addition of extra KOH used during chemical activation.

In AC electrodes, O has been identified as a natural doping heteroatom that could produce a pseudo-capacitance effect in the electrochemical process in supercapacitors [42]. This was proven through electrochemical testing of the CV method with deviations in the electric double-layer capacitance (EDLC) produced from 0.5-YBAC electrodes, resulting in a higher C_{sp} [43]. Moreover, the S element in the 0.5-YBAC sample verified its wettability properties, indicating the sample's ideal circumstances.

SEM analysis showed the morphological structure of YBAC samples at the nanometer scale with a dark-light pattern visible at a resolution of 5000x and 15000x as shown in Figure 3. The characterization results

were processed using IC measure software to obtain the size of the surface pore diameter. 0.3-YBAC had a morphological structure similar to the distribution of a black hole, with a larger particle size (273-743 nm), which was classified as a pore, see Figures 3(a) and 3(b). Conversely, 0.5-YBAC samples had a surface structure with smaller particles (18-229 nm) and pores with particle sizes ranging from 45-176 nm, Figure 3(c). This indicated that the smaller particle size and higher pore density resulted in enhanced SSA, C_{sp} , and specific energy [30]. When examined at 15000x magnification, 0.5-YBAC samples had a 3D hierarchical pore structure with tunnel-like pores. The presence of abundant hierarchical pores at a nanometer scale was suitable for efficient charge storage [44]. Figure 3(d) clearly provided the tunnel-like pore shape, with the presence of holes leading into the surface of carbon samples, indicating that electrolyte ions would have smooth access to the electrode pores. It was observed that improved ion accessibility resulted in higher power output [45]. The morphology of the 0.7-YBAC sample showed the presence of irregular carbon particles with fewer pores and larger particle sizes ranging from 213-416 nm. Additionally, the SEM appearance of the sample showed the collapse of pores due to the addition of activator concentrations that exceeded the optimum conditions. This high concentration eroded and collapsed the previously optimal pore structure, as provided in Figure 3(e) and Figure 3(f), resulting in fewer accessible pores and reduced physical-chemical characteristics.

Table 1. Microcrystalline dimension data and chemical element composition of YBAC samples for each variation of chemical activating agent concentration

Sample	$2\theta_{002}$	$2\theta_{100}$	d_{002}	d_{100}	L_c	L_a	Chemical compound (%)						
	(°)	(°)	(Å)	(Å)	(Å)	(Å)	C	O	S	K	Zn	Na	Si
0.3-YBAC	22.08	44.05	4.02	2.05	9.73	29.67	82.94	4.23	5.36	0.20	7.28	-	-
0.5-YBAC	22.96	43.69	3.87	2.07	7.37	18.99	89.16	10.14	0.10	0.29	-	0.31	-
0.7-YBAC	22.27	43.08	3.99	2.09	10.86	21.91	89.89	9.45	-	0.31	-	0.25	0.10

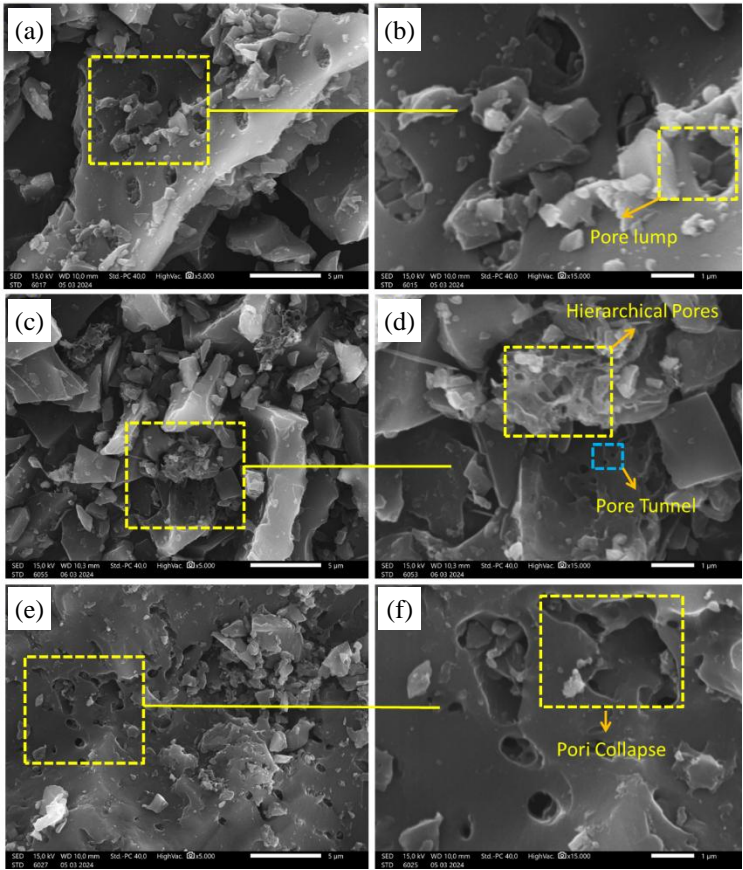


Figure 3. SEM morphological view of (a) 0.3-YBAC at 5000x resolution, (b) 0.3-YBAC at 40000x resolution, (c) 0.5-YBAC at 5000x resolution, (d) 0.5-YBAC at 40000x resolution, (e) 0.7-YBAC at 5000x resolution, and (f) 0.7-YBAC at 40000x resolution

A more detailed analysis of the porosity of the YBAC sample, including the SSA, pore volume, and distribution, was thoroughly examined using the characterization of N₂ gas absorption. The analysis of porosity was critical in the prediction of increasing C_{sp}, energy density, and power density. The SSA of YBAC was determined using the BET method, while its pore distribution was determined through the DFT. N₂ gas adsorption-desorption measurements were visualized through the isotherm curve of the relationship between the STP absorption volume (cm³ g⁻¹) and the relative pressure (P P₀⁻¹) for each sample, as shown in Figure 4. The isotherm measurement results showed that the BET curve matched the IUPAC categorization of Type IV hysteresis (H1 and H4). This was in accordance with the analysis of N₂ gas absorption shown at low relative pressure (P P₀⁻¹ < 0.3), signifying the availability of dominant micropores. The absorption at higher pressures (0.4 < P P₀⁻¹ < 0.9) and the production of a significant H4 hysteresis loop indicated the presence of mesopores. Meanwhile, adsorption at relatively higher pressure (P P₀⁻¹ > 0.9) indicated the presence of macropores.

The adsorption volume corresponded to the number of pores that supported the availability of higher SSA, as presented in Table 2 [28]. The test results of the 0.3-YBAC sample showed an adsorption volume of 63.28 cm³ g⁻¹ with an SSA of around 367.55 m² g⁻¹. After the addition of KOH reagent to the 0.5-YBAC sample, there was a significant increase in adsorption volume, reaching 93.97 cm³ g⁻¹, as indicated by the higher pressure produced. This increase resulted in an SSA of 422 m² g⁻¹ for the 0.5-YBAC sample. Adding more KOH to the 0.7-YBAC sample reduced the adsorption volume to 92.29 cm³ g⁻¹ and the SSA to 350.10 m² g⁻¹. The pore distribution in YBAC samples was dominated by micro and mesopores that were uniformly distributed across the surface of the material. Micropores dominated the 0.3-YBAC sample, accounting for 0.35 cm³ nm⁻¹ g⁻¹, while mesopores contributed less than 0.1 cm³ nm⁻¹ g⁻¹. The SSA of micropores reached 335 m² g⁻¹, whereas mesopores contributed 32.54 m² g⁻¹. It was also observed that the 0.5-YBAC sample showed a significant increase in micro and mesopores. The micropore volume reached 2.8 cm³ nm⁻¹ g⁻¹, while the mesopore volume increased to 0.5 cm³ nm⁻¹ g⁻¹. These results correlated with the increasing SSA of micropores and mesopores, which were 377.3 m² g⁻¹ and 44.72 m² g⁻¹, respectively. In the 0.7-YBAC sample, micropores and mesopore volumes decreased to 2.3 cm³ nm⁻¹ g⁻¹ and 0.2 cm³ nm⁻¹ g⁻¹ with the SSA of 304.3 m² g⁻¹ and 45.82 m² g⁻¹, respectively. The optimization of micropore formation in YBAC samples was supported through the use of chemical reagents. Under high temperatures, C reacted with KOH, causing the release of K bonds in the carbon chain and facilitating the production of micropores in the carbon particle structure. This analysis was in line with the isotherm curve data, which showed the availability of dominant micro-mesopores. The presence of optimal micro-mesopores in the 0.5-YBAC sample supported the performance of supercapacitor cell electrodes [46]. Moreover, the existence of smaller micropores facilitated ion storage, resulting in higher energy density in the 0.5-YBAC sample. The availability of mesopores helped increase the speed of ion transport by reducing the distance between pores and the surface of C electrodes, leading to higher power density [47].

Table 2. Pores structure parameters of N₂ gas absorption on biomass-based AC

Sample	Activating agent	pyrolysis	Morphology	S _{BET} (m ² g ⁻¹)	S _{mic} (m ² g ⁻¹)	S _{mes} (m ² g ⁻¹)	V _{tot} (cm ³ g ⁻¹)	D _{ave} (nm)	Ref.
Shea butter	1:0.5 KOH	N ₂	Hierarchical	1016.2	846.3	169.9	0.42	4.4	[48]
Candlenut shells	NaOH	-	Diverse pores	60.88	-	-	0.33	25.63	[36]
Hippophae rhamnoides fruit	KOH	N ₂	Hierarchical	787.05	-	-	0.38	1.35	[49]
Turmeric leaves	KOH	Ar	Hierarchical	541	418	123	0.47	-	[50]
mushroom substrate	KOH	N ₂	Roughness	2169	-	-	1.65	-	[51]
Marigold flower	ZnCl ₂	N ₂	Smooth and layered texture	664.6	505.6	158.91	0.35	-	[52]
0.3-YBAC	0.3 M KOH	N ₂ -CO ₂	Hierarchical	367.55	335.00	32.54	0.243	2.64	This research
0.5-YBAC	0.5 M KOH			422.00	377.30	44.72	0.287	2.70	
0.7-YBAC	0.7 M KOH			350.10	304.30	45.82	0.253	2.88	

The electrochemical properties of YBAC samples were evaluated using CV to determine C_{sp}, energy, and power. The test data were processed using the SigmaPlot 1.5 application to visualize the relationship curve of current density and voltage at scan rate variations of 1, 2, and 5 mV s⁻¹, with a potential window of 0-1000 mV. The CV curve, which resembled an imperfect rectangle, showed the electrode charging-discharging process, verifying the EDLC nature with pseudo-capacitance of 0.5-YBAC electrodes [53]. During the charging process, the current increased as the voltage moved toward the maximum state (0-1000 mV), forcing ions from the decomposed electrolyte to move toward the opposite pole to fill the pores in YBAC electrodes [54]. The discharge process occurred when the voltage reached zero (1000-0 mV), causing the ions stored in the pores to leave the electrodes. The area under the CV curve represented the size of the C_{sp} value. Figure 5 provided that 0.3-YBAC sample had the lowest C_{sp} value due to the small influence of the 0.3 M KOH reagent concentration. In contrast, the 0.5-YBAC sample had the highest C_{sp} and slightly prominent peaks in the CV

curve, indicating the presence of pseudo-capacitance, which increased the maximization of capacitance in testing electrochemical properties. Pseudo-capacitance was generated from the availability of self-doping of O and S heteroatoms, which supported the occurrence of redox reactions during electrochemical testing, as shown by EDS analysis. This method presented the C_{sp} values for the 3 YBAC electrodes with varying KOH reagent concentrations. 0.3-YBAC, 0.5-YBAC, and 0.7-YBAC samples had a C_{sp} value of 20 F g⁻¹, 175 F g⁻¹ and, 139 F g⁻¹, respectively. The resulting C_{sp} value decreased with the addition of KOH concentration due to the collapse of the previously optimal pores. The reduction was supported by a decrease in O and S content in the electrode material, as evidenced by SEM, EDS, and N₂ gas adsorption characterizations. Moreover, the EDLC properties of the YBAC supercapacitor sample were reviewed at different scan rates using the CV method. The results showed that the scan rate greatly affected the shape of the EDLC. At high scan speeds, all 3 electrodes showed almost perfect rectangular curves, indicating a more dominant EDLC property. However, the application of high scan rates could reduce the C_{sp} of each electrode by reducing the opportunity for ions to fill the pores of the electrode. The best scan rate (1 mV s⁻¹) provided an extended time for ions to fill the pores spread on the electrode surface, indicating a higher C_{sp} value [55].

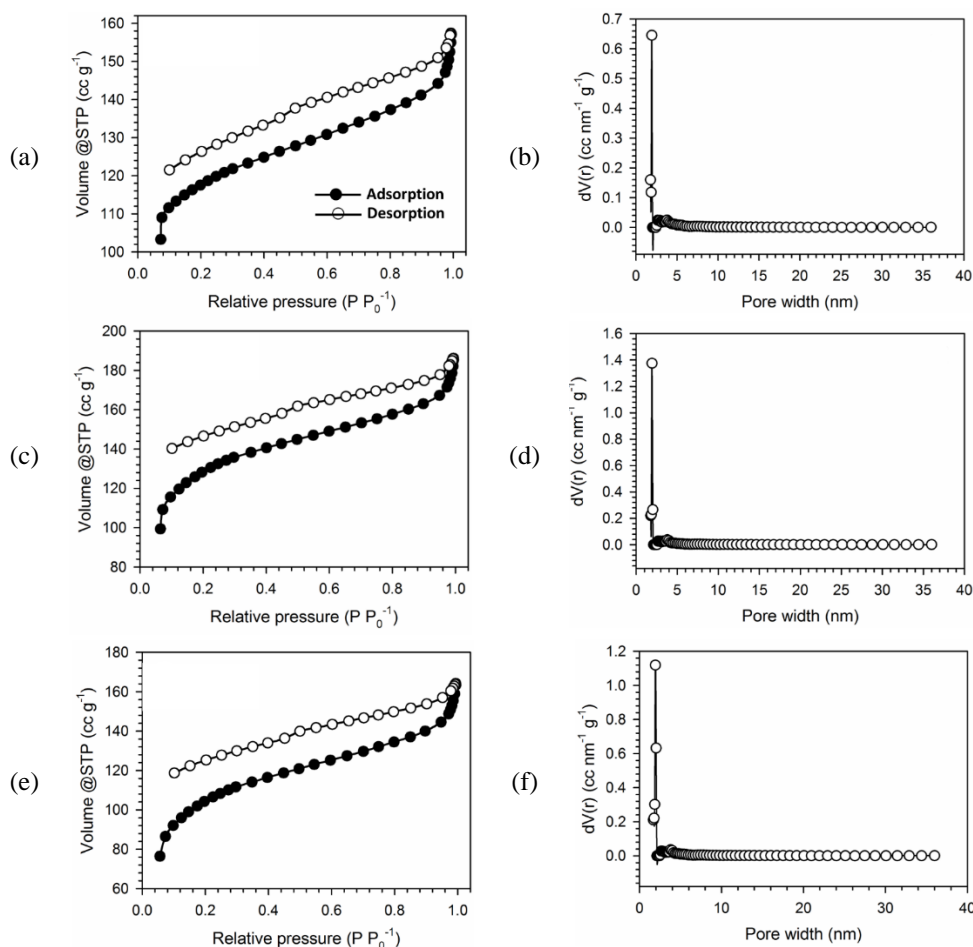


Figure 4. N₂ gas absorption capacity for (a) 0.3-YBAC isotherm curve, (b) 0.3-YBAC DFT curve, (c) 0.5-YBAC isotherm curve, (d) 0.5-YBAC DFT curve, (e) 0.7-YBAC isotherm curve, and (f) 0.7-YBAC DFT curve

The electrochemical activity of YBAC samples was further examined using the GCD method to validate the CV results with more complex measurement parameters. Figure 6 presents the visualization of the comparative GCD output at a current density of 1 A g⁻¹. It was observed that the 0.5-YBAC sample had the highest charge-discharge time response, with the curve shape creating an imperfect isosceles triangle and non-linear characteristics of the voltage time [56]. This resulted in the highest C_{sp} of 214 F g⁻¹ (Figure 6(a)) in an acidic electrolyte (1 M H₂SO₄). Meanwhile, the electrodes of 0.3-YBAC and 0.7-YBAC samples had lower C_{sp} values of 73 F g⁻¹ and 157 F g⁻¹, respectively. The lower values were due to the suboptimal pore formation

and collapse of the porous structure, as well as the presence of natural doping elements O and S that were not suitable for increasing the C_{sp} value.

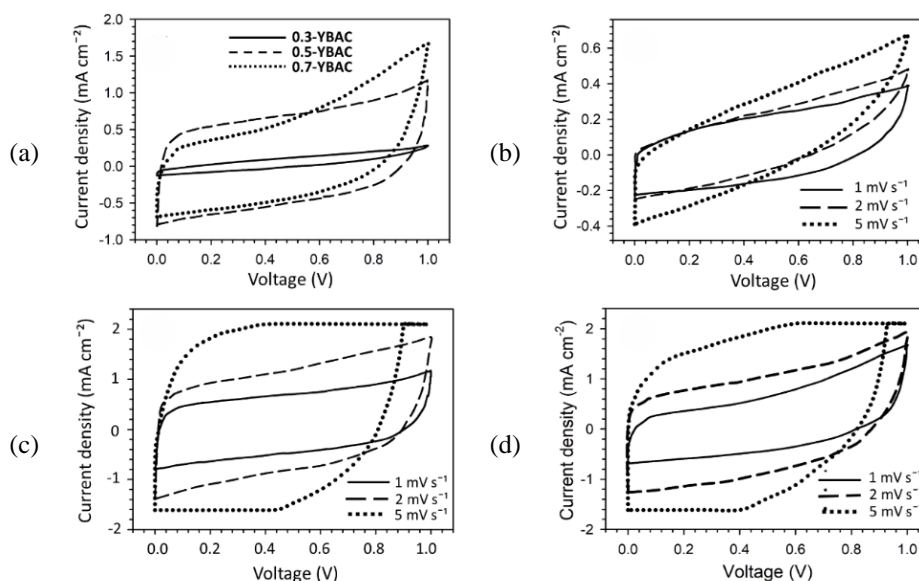


Figure 5. CV curves at the same and different scan rates for (a) all samples, (b) 0.3-YBAC, (c) 0.5-YBAC, and (d) 0.7-YBAC

The GCD profiles of supercapacitor cells assembled with symmetric electrodes shaped at various current densities, Figures 6(b)-6(d), indicated an isosceles triangle shape with an extended time, which could be maintained properly to a high current density of 10 A g^{-1} . The highest C_{sp} for the 0.5-YBAC sample of 214 F g^{-1} was achieved at 1 A g^{-1} due to the maximization of the fast ion transport time through the 3D hierarchical nanopores structure, such as the pore tunnel. The rapid voltage drop when entering the discharging process represented the internal resistance of the electrode material. Additionally, the 0.5-YBAC sample showed the smallest IR drop, indicating the best conductivity. The R_c values for 0.3-YBAC, 0.5-YBAC, and 0.7-YBAC were calculated for electrode materials as 3.62, 2.72, and 4.95Ω , respectively. Based on the results of each characterization, 0.5-YBAC samples showed the availability of charge distribution access by H^+ and SO_4^{2-} ions, which were smoother across the electrode interface pores with a 3D hierarchical micro-meso structure [57]. The existence of optimal self-doping of S and O heteroatoms bound in the C framework could induce pseudo-capacitance of electrode materials. This resulted in a current increase at a certain voltage during the electrochemical process, leading to the enhancement of C_{sp} , conductivity, and wettability of the material [58]. In addition, amorphous porosity with a structure such as a pore tunnel supported the SSA and the amount of pore volume to reduce the resistance of the material on the electrode's surface. It was reported that 0.5-YBAC supercapacitor cell electrodes had a C_{sp} value competitive with other biomass waste-based electrodes, Figure 6(e) and Table 3. YB played a crucial role in making C electrodes for supercapacitor cells that were influenced by KOH reagent with a concentration of 0.5 M, suggesting a capacitance performance reaching 214 F g^{-1} . The analysis was also strengthened by the output of SEM and EDS characterization. Furthermore, a review of the Ragone plot, Figure 6(f) provided the maximum E_{sp} of 24.7 Wh kg^{-1} and P_{sp} of 119.2 W kg^{-1} .

Table 3. Comparison of C_{sp} values of C electrodes from various biomasses

Sample	Doping	Electrolyte	Current (A g^{-1})	C_{sp} (F g^{-1})	E_{sp} (Wh kg^{-1})	P_{sp} (W kg^{-1})	R (Ω)	Ref.
Distiller's grains	N,O	6 M KOH	1	345.2	12.2	348.8	1.837	[59]
Coconut shell	N,B	2 M ZnSO_4	0.25	72	139.46	355.81	3.02	[16]
Garlic peels	N,O	6 M KOH	25	283.13	9.07	309.2	0.681	[14]
Faidherbia Albida	N, P, S	3 M KOH	1.4	109.1	54.7	1080	-	[60]
Wood waste	-	6 M KOH	3	183.4	4.2	137	-	[39]
Fabaceae-Plants	-	6 M KOH	0.5	279	14.15	50	1.13	[61]
0.5-YBAC	O,S	H_2SO_4	1	214	24.7	119.2	2.72	This work

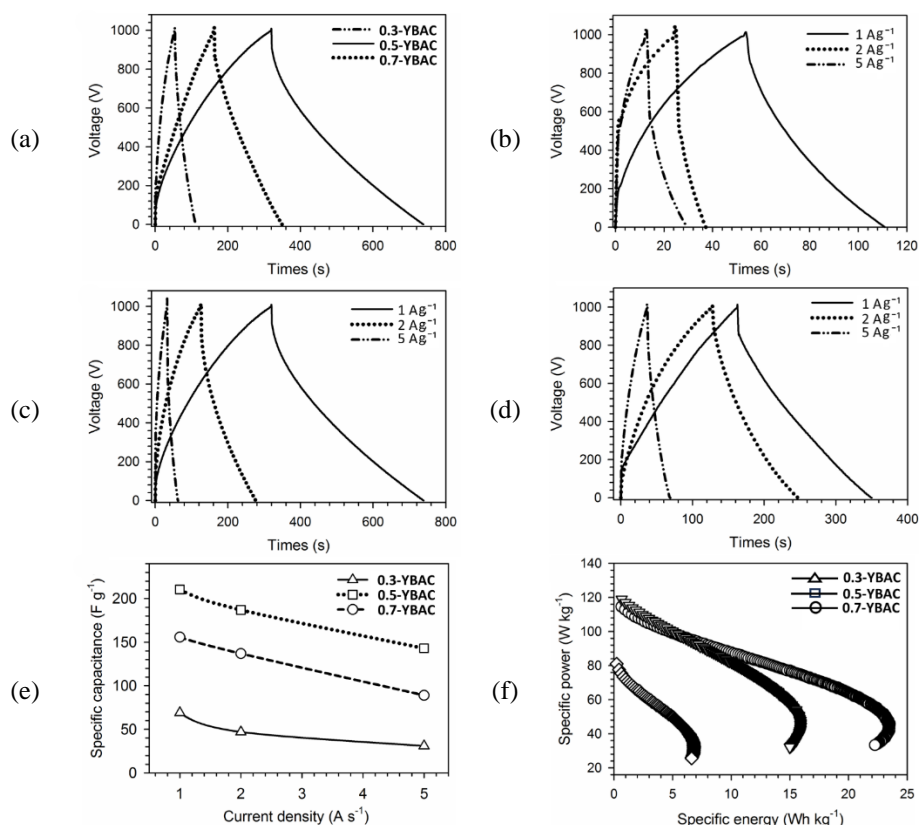


Figure 6. GCD curves at current densities of (a) 1 A; (b) 0.3-YBAC at 1A, 2A, and 5A; (c) 0.5-YBAC at 1A, 2A, and 5A; (d) 0.7-YBAC at 1A, 2A, and 5A; (e) relationship of specific capacitance with current density; and (f) dragon plot for all variations of YBAC samples

4. CONCLUSION

In conclusion, YB stem waste was selected as a source of AC, which had a high porosity and 87% carbon purity, making it suitable for use as an electrode material in supercapacitors. The 3D hierarchical nanopores structure, characterized by inwardly forming tunnels, along with its amorphous-porosity properties and surface pore size distribution, was in accordance with the typical characteristics of biomass-based AC. All YBAC electrodes with different activator concentrations were tested for their storage capabilities using the same parameters under the influence of 1 M H₂SO₄ liquid electrolyte at a low scan rate of 1 mV s⁻¹. Among the electrodes, 0.5-YBAC showed the best condition, maintaining 88% of the initial C_{sp} of 214 F g⁻¹, which slightly decreased to 188 F g⁻¹ at a scan rate of 2 mV s⁻¹. As a result, this study showed that AC produced from YB stem waste could be used as the basic material for cathodes and anodes of supercapacitors with specific energy-power strengths reaching 24.7 Wh kg⁻¹ and 119.2 W kg⁻¹ with R_c 2.72 Ω.

FUNDING INFORMATION

The research was financially supported by First year Project of Fundamental-Regular (PFR) in Ministry of Education, Culture, Research, and Technology, Republic of Indonesia (*Kementerian Pendidikan, Kebudayaan, Riset, dan Teknologi, Republic of Indonesia*) with the title "Improving the practical performance of supercapacitors through natural structure-doping engineering on carbon, a natural material typical of Indonesia, as an energy storage for electric vehicles" contract No.: 19521/UN19.5.1.3/AL.04/2025.

AUTHOR CONTRIBUTIONS STATEMENT

This journal uses the Contributor Roles Taxonomy (CRediT) to recognize individual author contributions, reduce authorship disputes, and facilitate collaboration.

Name of Author	C	M	So	Va	Fo	I	R	D	O	E	Vi	Su	P	Fu
Erman Taer	✓	✓		✓	✓	✓		✓	✓	✓		✓	✓	✓
Novi Yanti		✓	✓	✓	✓	✓	✓	✓	✓	✓	✓		✓	
Rahma Lia Putri		✓	✓			✓	✓	✓	✓		✓			
Apriwandi Apriwandi				✓	✓	✓	✓	✓	✓		✓			
Awaludin Martin			✓		✓		✓	✓	✓		✓			
Julnaidi Julnaidi		✓	✓	✓		✓	✓	✓	✓		✓			
Nidya Chitraningrum		✓	✓			✓	✓		✓		✓	✓		
Ahmad Fudholi		✓	✓			✓	✓		✓		✓	✓		
Rika Taslim	✓	✓		✓	✓	✓		✓	✓	✓		✓	✓	

C : Conceptualization
M : Methodology
So : Software
Va : Validation
Fo : Formal analysis

I : Investigation
R : Resources
D : Data Curation
O : Writing - Original Draft
E : Writing - Review & Editing

Vi : Visualization
Su : Supervision
P : Project administration
Fu : Funding acquisition

CONFLICT OF INTEREST STATEMENT

The authors declare that they have no known competing financial interests or personal relationships that could have appeared to influence the work reported in this paper.

DATA AVAILABILITY

The data that support the findings of this study are available from the corresponding author, [ET], upon reasonable request.

REFERENCES

[1] H. Wang, F. Ruan, Q. Feng, Y. Liu, and H. Wang, "Preparation of biomass-derived activated carbon from golden needle mushroom roots for supercapacitor electrodes," *Materials Letters*, vol. 368, p. 136644, Aug. 2024, doi: 10.1016/j.matlet.2024.136644.

[2] H. Liu *et al.*, "Efficient conversion of biomass waste to N/O co-doped hierarchical porous carbon for high performance supercapacitors," *Journal of Analytical and Applied Pyrolysis*, vol. 169, p. 105844, Jan. 2023, doi: 10.1016/j.jaap.2022.105844.

[3] S. Ryan *et al.*, "Single walled carbon nanotube functionalisation in printed supercapacitor devices and shielding effect of Tin(II) Oxide," *Electrochimica Acta*, vol. 448, p. 142168, Apr. 2023, doi: 10.1016/j.electacta.2023.142168.

[4] E. Taer, L. Pratiwi, A. Apriwandi, W. S. Mustika, R. Taslim, and A. Agustino, "Three-dimensional pore structure of activated carbon monolithic derived from hierarchically bamboo stem for supercapacitor application," *Communications in Science and Technology*, vol. 5, no. 1, pp. 22–30, Jul. 2020, doi: 10.21924/cst.5.1.2020.180.

[5] A. Nandagudi *et al.*, "Porous potassium tantalate-reduced graphene oxide nano cube architecture for high performance hybrid supercapacitors," *e-Prime - Advances in Electrical Engineering, Electronics and Energy*, vol. 4, p. 100182, Jun. 2023, doi: 10.1016/j.prime.2023.100182.

[6] A. Husain *et al.*, "Harnessing sustainable N-doped activated carbon from walnut shells for advanced all-solid-state supercapacitors and targeted Rhodamine B dye adsorption," *Journal of Science: Advanced Materials and Devices*, vol. 9, no. 2, p. 100699, Jun. 2024, doi: 10.1016/j.jsamd.2024.100699.

[7] E. Taer *et al.*, "Meso- and microporous carbon electrode and its effect on the capacitive, energy and power properties of supercapacitor," *International Journal of Power Electronics and Drive Systems (IJPEDS)*, vol. 9, no. 3, pp. 1263-1271, Sep. 2018, doi: 10.11591/ijpeds.v9.i3.pp1263-1271.

[8] Z.-W. Zhang *et al.*, "Self-assembly of caragana-based nanomaterials into multiple heteroatom-doped 3D-interconnected porous carbon for advanced supercapacitors," *Materials Today Advances*, vol. 19, p. 100394, Aug. 2023, doi: 10.1016/j.mtadv.2023.100394.

[9] Z. Chen *et al.*, "Molecularly-regulating oxygen-containing functional groups of ramie activated carbon for high-performance supercapacitors," *Journal of Colloid and Interface Science*, vol. 665, pp. 772–779, Jul. 2024, doi: 10.1016/j.jcis.2024.03.177.

[10] S. Peng *et al.*, "Hierarchical rapeseed stalk-derived activated carbon porous structure with N and O codoping for symmetric supercapacitor," *Colloids and Surfaces A: Physicochemical and Engineering Aspects*, vol. 688, p. 133666, May 2024, doi: 10.1016/j.colsurfa.2024.133666.

[11] Y. Li and B. Qi, "Secondary utilization of jujube shell bio-waste into biomass carbon for supercapacitor electrode materials study," *Electrochemistry Communications*, vol. 152, p. 107512, Jul. 2023, doi: 10.1016/j.elecom.2023.107512.

[12] R. Sun *et al.*, "Sodium lignosulfonate-derived hierarchical porous carbon electrode materials for supercapacitor applications," *Journal of Energy Storage*, vol. 91, 2024, doi: 10.1016/j.est.2024.112025.

[13] G. Li, S. Chen, Y. Wang, G. Wang, Y. Wu, and Y. Xu, "N, S co-doped porous graphene-like carbon synthesized by a facile coal tar pitch-blowing strategy for high-performance supercapacitors," *Chemical Physics Letters*, vol. 827, 2023, doi: 10.1016/j.cpl.2023.140712.

[14] S. Liu *et al.*, "Facile and green synthesis of biomass-derived N, O-doped hierarchical porous carbons for high-performance supercapacitor application," *Journal of Analytical and Applied Pyrolysis*, vol. 177, Jan. 2024, doi: 10.1016/j.jaap.2023.106278.

[15] Z. Asadi Ghare Jeloo *et al.*, "From barley straw biomass to N/S co-doped as electrode material for high-performance supercapacitor applications," *Materials Chemistry and Physics*, vol. 323, 2024, doi: 10.1016/j.matchemphys.2024.129653.




[16] D. Zhang, X. Zhan, T. Zhou, J. Du, K. Zou, and Y. Luo, "N/B co-doped porous carbon with superior specific surface area derived from activation of biomass waste by novel deep eutectic solvents for Zn-ion hybrid supercapacitors," *Journal of Materials Science and Technology*, vol. 193, pp. 22–28, 2024, doi: 10.1016/j.jmst.2024.01.019.

- [17] H. Y. Choi, B. M. Lee, and Y. G. Jeong, "Microstructures and electrochemical characterization of graphene oxide/carboxymethylated cellulose nanofibril-derived hybrid carbon aerogels for freestanding supercapacitor electrodes," *International Journal of Electrochemical Science*, vol. 18, no. 5, 2023, doi: 10.1016/j.ijoes.2023.100101.
- [18] S. Rawat, R. K. Mishra, and T. Bhaskar, "Biomass derived functional carbon materials for supercapacitor applications," *Chemosphere*, vol. 286, 2022, doi: 10.1016/j.chemosphere.2021.131961.
- [19] B. Shaku, T. P. Mofokeng, N. J. Coville, K. I. Ozoemena, and M. S. Maubane-Nkadimeng, "Biomass valorisation of marula nutshell waste into nitrogen-doped activated carbon for use in high performance supercapacitors," *Electrochimica Acta*, vol. 442, 2023, doi: 10.1016/j.electacta.2023.141828.
- [20] Y. Zhang, S. Hui, X. Lin, Z. Ying, Y. Li, and J. Xie, "Novel effective strategy for high-performance biomass-based super-flexible hierarchically porous carbon fibrous film electrode for supercapacitors," *Journal of Alloys and Compounds*, vol. 883, 2021, doi: 10.1016/j.jallcom.2021.160713.
- [21] B. Wang, L. Ji, Y. Yu, N. Wang, J. Wang, and J. Zhao, "A simple and universal method for preparing N, S co-doped biomass derived carbon with superior performance in supercapacitors," *Electrochimica Acta*, vol. 309, 2019, doi: 10.1016/j.electacta.2019.04.087.
- [22] N. Gunasekaran, M. Shanmugaraja, R. Bharathwaaj, J. Shilpha Dharshini, M. Vivishnu Kumar, and P. S. Yogesh Kumar, "Analysis and reduction of heat transfer in a furnace of refinery," *Journal of Physics: Conference Series*, vol. 1706, no. 1, p. 012176, Dec. 2020, doi: 10.1088/1742-6596/1706/1/012176.
- [23] X. Yang *et al.*, "Preparation of biomass-based N, P, and S co-doped porous carbon with high mesoporosity based on the synergistic effect of NaOH/thiourea and melamine phosphate and its application in high performance supercapacitors," *Journal of Analytical and Applied Pyrolysis*, vol. 169, 2023, doi: 10.1016/j.jaap.2022.105822.
- [24] W. Yue, Z. Yu, X. Zhang, H. Liu, T. He, and X. Ma, "Green activation method and natural N/O/S co-doped strategy to prepare biomass-derived graded porous carbon for supercapacitors," *Journal of Analytical and Applied Pyrolysis*, vol. 178, 2024, doi: 10.1016/j.jaap.2024.106409.
- [25] W. Yue, Z. Yu, X. Zhang, H. Liu, Y. Zhang, and X. Ma, "Preparation of natural N/O/S co-doped biomass-derived carbon materials for supercapacitors using multistage gas self-exfoliation effect," *Journal of Analytical and Applied Pyrolysis*, vol. 179, 2024, doi: 10.1016/j.jaap.2024.106525.
- [26] R. Farma *et al.*, "Enhanced electrochemical performance of oxygen, nitrogen, and sulfur trial-doped Nypa fruticans-based carbon nanofiber for high performance supercapacitors," *Journal of Energy Storage*, vol. 67, 2023, doi: 10.1016/j.est.2023.107611.
- [27] N. A. Echeverry-Montoya, J. J. Prias-Barragán, L. Tirado-Mejía, C. Agudelo, G. Fonthal, and H. Ariza-Calderón, "Fabrication and electrical response of flexible supercapacitor based on activated carbon from bamboo," *Physica Status Solidi C*, vol. 14, no. 3–4, Mar. 2017, doi: 10.1002/pssc.201600258.
- [28] M. Jalalah, A. K. Nayak, and F. A. Harraz, "Eco-friendly preparation of nitrogen-doped porous carbon materials for enhanced solid-state supercapacitor device," *Diamond and Related Materials*, vol. 147, p. 111264, Aug. 2024, doi: 10.1016/j.diamond.2024.111264.
- [29] T. Kongthong *et al.*, "Microwave-assisted synthesis of nitrogen-doped pineapple leaf fiber-derived activated carbon with manganese dioxide nanofibers for high-performance coin- and pouch-cell supercapacitors," *Journal of Science: Advanced Materials and Devices*, vol. 7, no. 2, p. 100434, Jun. 2022, doi: 10.1016/j.jsamd.2022.100434.
- [30] E. Taer, N. Yanti, J. A. Putri, A. Apriwandi, and R. Taslim, "Novel macaroni-sponge-like pore structure biomass (Zingiber officinale Rosc. leaves)-based electrode material for excellent energy gravimetric supercapacitor," *Journal of Chemical Technology and Biotechnology*, vol. 98, no. 4, pp. 990–1002, 2023, doi: 10.1002/jctb.7303.
- [31] A. Sandeep, P. T, and A. V. Ravindra, "Activated carbon derived from corncob via hydrothermal carbonization as a promising electrode for supercapacitors," *Materials Research Bulletin*, vol. 179, p. 112991, Nov. 2024, doi: 10.1016/j.materresbull.2024.112991.
- [32] Z. Yao, B. Quan, T. Yang, J. Li, and C. Gu, "Flexible supercapacitors based on vertical graphene/carbon fabric with high rate performance," *Applied Surface Science*, vol. 610, p. 155535, Feb. 2023, doi: 10.1016/j.apsusc.2022.155535.
- [33] L. Wang, W. Li, P. Li, L. Zhang, and L. Li, "KHCO₃ chemical-activated hydrothermal porous carbon derived from jackfruit inner skin for supercapacitor applications," *Journal of Molecular Structure*, vol. 1318, 2024, doi: 10.1016/j.molstruc.2024.139380.
- [34] G. Yirdaw, A. Dessie, and T. A. Birhan, "Optimization of process variables to prepare activated carbon from Noug (Guizotia abyssinica cass.) stalk using response surface methodology," *Heliyon*, vol. 9, no. 6, 2023, doi: 10.1016/j.heliyon.2023.e17254.
- [35] A. Husain *et al.*, "Harnessing sustainable N-doped activated carbon from walnut shells for advanced all-solid-state supercapacitors and targeted Rhodamine B dye adsorption," *Journal of Science: Advanced Materials and Devices*, vol. 9, no. 2, p. 100699, Jun. 2024, doi: 10.1016/j.jsamd.2024.100699.
- [36] M. Hamid, N. Haida Mohd Kaus, S. Humaidi, I. Isnaeni, A. Daulay, and I. Revita Saragi, "Activated carbon from biomass waste candlenut shells (Aleurites moluccana) doped ZIF-67/Fe₃O₄ as advanced materials for supercapacitor," *Materials Science for Energy Technologies*, vol. 7, pp. 381–390, 2024, doi: 10.1016/j.mset.2024.07.004.
- [37] M. Honarmand, A. Naeimi, M. S. Rezakhani, and M. A. Chaji, "Ni/NiO doped chitosan-cellulose based on the wastes of barley and shrimp for degradation of ciprofloxacin antibiotic," *Journal of Materials Research and Technology*, vol. 18, pp. 4060–4074, May 2022, doi: 10.1016/j.jmrt.2022.04.046.
- [38] N. Boonraksa, E. Swatsitang, and K. Wongsaprom, "Biomass nanoarchitectonics with activated rice husk char for nanoporous carbon as electrode material: Enhancing supercapacitor electrochemical performance," *Journal of Non-Crystalline Solids*, vol. 637, 2024, doi: 10.1016/j.jnoncrysol.2024.123064.
- [39] D. Shrestha, "Structural and electrochemical evaluation of renewable carbons and their composites on different carbonization temperatures for supercapacitor applications," *Heliyon*, vol. 10, no. 4, 2024, doi: 10.1016/j.heliyon.2024.e25628.
- [40] R. Yuksel and N. Karakehya, "High energy density biomass-derived activated carbon materials for sustainable energy storage," *Carbon*, vol. 221, p. 118934, Mar. 2024, doi: 10.1016/j.carbon.2024.118934.
- [41] J. Wang *et al.*, "Preparation and application of biomass-based porous carbon with S, N, Zn, and Fe heteroatoms loading for use in supercapacitors," *Biomass and Bioenergy*, vol. 156, p. 106301, Jan. 2022, doi: 10.1016/j.biombioe.2021.106301.
- [42] S. Lu *et al.*, "Multi-heteroatom-doped porous carbon with high surface adsorption energy of potassium derived from biomass waste for high-performance supercapacitors," *International Journal of Biological Macromolecules*, vol. 258, 2024, doi: 10.1016/j.ijbiomac.2023.128794.
- [43] G. Wang, M. Guan, R. Fu, C. Yong, Y. Zhu, and L. Pan, "Fermentation-hot pressing assisted preparation of bamboo green-activated carbon for supercapacitors," *Diamond and Related Materials*, vol. 143, 2024, doi: 10.1016/j.diamond.2024.110871.
- [44] J. Zhang, Y. Cao, W. Zhou, and H. Chai, "Fabrication of solid-state high capacitance supercapacitor from N-doped biomass porous carbon," *Diamond and Related Materials*, vol. 141, p. 110612, Jan. 2024, doi: 10.1016/j.diamond.2023.110612.
- [45] N. Toyama *et al.*, "Enhanced activity for reduction of 4-nitrophenol of Ni/single-walled carbon nanotube prepared by super-growth method," *Nanotechnology*, vol. 33, no. 6, 2022, doi: 10.1088/1361-6528/ac353f.




- [46] J. Hu *et al.*, "Chitosan-derived large surface area porous carbon via microphase separation engineering of pore-regulation and nitrogen-doping coupling for high-performance supercapacitors," *Renewable Energy*, vol. 228, 2024, doi: 10.1016/j.renene.2024.120598.
- [47] L. H. Quan, U. T. Dieu Thuy, P. V. Nam, N. Van Chi, T. X. Duong, and N. Van Hoa, "Chitosan-derived carbon aerogel nanocomposite as an active electrode material for high-performance supercapacitors," *Journal of Science: Advanced Materials and Devices*, vol. 8, no. 3, 2023, doi: 10.1016/j.jsamd.2023.100586.
- [48] D. Nframah Ampong *et al.*, "Utilization of shea butter waste-derived hierarchical activated carbon for high-performance supercapacitor applications," *Bioresource Technology*, vol. 406, p. 131039, Aug. 2024, doi: 10.1016/j.biortech.2024.131039.
- [49] Z. Bian *et al.*, "Converting Hippophae rhamnoides fruit extraction residue into porous carbons with ultra-high surface area for superior-performance supercapacitors," *Journal of Energy Storage*, vol. 98, p. 113058, Sep. 2024, doi: 10.1016/j.est.2024.113058.
- [50] R. Chakraborty *et al.*, "Nitrogen and oxygen self-doped hierarchical porous carbon nanosheets derived from turmeric leaves for high-performance supercapacitor," *Inorganica Chimica Acta*, vol. 567, p. 122056, Jul. 2024, doi: 10.1016/j.ica.2024.122056.
- [51] N. Boulanger, A. V. Talyzin, S. Xiong, M. Hultberg, and A. Grimm, "High surface area activated carbon prepared from wood-based spent mushroom substrate for supercapacitors and water treatment," *Colloids and Surfaces A: Physicochemical and Engineering Aspects*, vol. 680, 2024, doi: 10.1016/j.colsurfa.2023.132684.
- [52] R. Jangra *et al.*, "ZnCl₂-assisted conversion of nitrogen-containing biomass carbon from marigold flower: Toward highly porous activated nitrogen-doped carbon for low ESR and enhanced energy density supercapacitors," *Journal of Energy Storage*, vol. 75, 2024, doi: 10.1016/j.est.2023.109728.
- [53] M. Hamid *et al.*, "Sweet potato-derived carbon nanosheets incorporate NiCo₂O₄ nanocomposite as electrode materials for supercapacitors," *Materials Science for Energy Technologies*, vol. 6, pp. 382–387, 2023, doi: 10.1016/j.mset.2023.03.006.
- [54] D. S. Priya, L. J. Kennedy, and G. T. Anand, "Effective conversion of waste banana bract into porous carbon electrode for supercapacitor energy storage applications," *Results in Surfaces and Interfaces*, vol. 10, 2023, doi: 10.1016/j.rsufi.2023.100096.
- [55] S. R. A. Sasono, M. F. Rois, W. Widiyastuti, T. Nurtono, and H. Setyawan, "Nanofiber-enrich dispersed activated carbon derived from coconut shell for supercapacitor material," *Results in Engineering*, vol. 18, 2023, doi: 10.1016/j.rineng.2023.101070.
- [56] E. Taer *et al.*, "Aromatic biomass (torch ginger) leaf-derived three-dimensional honeycomb-like carbon to enhance gravimetric supercapacitor," *Journal of the Science of Food and Agriculture*, vol. 103, no. 15, pp. 7411–7423, Dec. 2023, doi: 10.1002/jsfa.12846.
- [57] S. C. Hu *et al.*, "Structural changes and electrochemical properties of lacquer wood activated carbon prepared by phosphoric acid-chemical activation for supercapacitor applications," *Renewable Energy*, vol. 177, Nov. 2021, doi: 10.1016/j.renene.2021.05.113.
- [58] R. Taslim, A. Apriwandi, and E. Taer, "Novel Moringa oleifera Leaves 3D Porous Carbon-Based Electrode Material as a High-Performance EDLC Supercapacitor," *ACS Omega*, vol. 7, no. 41, pp. 36489–36502, Oct. 2022, doi: 10.1021/acsomega.2c04301.
- [59] R. Han *et al.*, "N, O self-doped porous carbon derived from distiller's grains for high performance supercapacitors," *Industrial Crops and Products*, vol. 214, p. 118550, Aug. 2024, doi: 10.1016/j.indcrop.2024.118550.
- [60] A. A. Mohammed, J. K. Das, A. Hota, and B. C. Tripathy, "Facile synthesis of NiMoO₄@MnO₂ nanoflower and waste biomass-derived N, P, and S self-doped carbon for advanced asymmetric supercapacitor electrode materials," *Diamond and Related Materials*, vol. 144, 2024, doi: 10.1016/j.diamond.2024.110940.
- [61] C. Song, K. Han, Z. Teng, M. Wang, Y. Pei, and J. Liu, "Low metal content and hierarchically porous structure of 'Fabaceae-Plants' derived activated carbon for high-performance supercapacitors," *Journal of Energy Storage*, vol. 87, 2024, doi: 10.1016/j.est.2024.111430.

BIOGRAPHIES OF AUTHORS






Erman Taer    is a lecturer in Department of Physics at the Universitas Riau (UNRI), Riau, Indonesia. The fields of education that have been taken are Bachelor of Physics from Riau University, Master of Physics from Bandung Institute of Technology, Doctorate from National University of Malaysia, and received the title of professor in 2019. Became a Lecturer since 1995 with courses in basic physics, statistical physics, material characterization, classical mechanics I and II, reviewer LPPM University of Riau, Head of Physics Department. Writing in various national and international journals indexed by Scopus, and has several patent copyrights. He can be contacted at email: erman.taer@lecturer.unri.ac.id.






Novi Yanti    is a research assistant in the Physics Department of the University of Riau (UNRI), Riau, Indonesia. Her educational field is Bachelor of Physics at the University of Riau (UNRI) in 2016-2020 and continued her master's degree in physics at the University of Riau (UNRI) in 2021-2023. She can be contacted at email: yanti.novi2610@gmail.com.






Rahma Lia Putri    is a Bachelor of Physics student at the University of Riau (UNRI). The field of education that has been taken is S-1 Physics FMIPA, University of Riau from 2019 to 2023. She can be contacted at email: rahma.lia0326@student.unri.ac.id.






Apriwandi Apriwandi    is a lecturer in the Physics Department at the University of Riau (UNRI), Riau, Indonesia. The fields of education that have been taken are Bachelor of Physics from Riau University, Master of Physics from Riau University. Became a Lecturer in 2023 with courses in thermodynamics, electronics, acoustics, and literature seminars. Writing in various national and international journals indexed by Scopus, and has several patents and copyrights. His educational field is Bachelor of Physics at the University of Riau (UNRI) from 2013-2017, and he continued his master's degree in physics at the University of Riau (UNRI) from 2019 to 2021. He can be contacted at email: apriwandi@lecturer.unri.ac.id.






Awaludin Martin    is a lecturer in the Mechanical Engineering Department at the University of Riau (UNRI), Riau, Indonesia. The fields of education that have been taken are Bachelor of Physics from Mercubuana University, Master of Energy Conversion from Universitas Indonesia, Doctorate from Universitas Indonesia of Indonesia, and received the title of Professor in 2023. Became a lecturer with courses in material engineering, material strength mechanics, machine element design, production process, machine drawing and CAD, introduction to electricity and electromagnetism, and head of the mechanical engineering department. Writing in various national and international journals indexed by Scopus, and has several patents and copyrights. He can be contacted at email: awaludinmartin@lecturer.unri.ac.id.






Julnaidi Julnaidi    is a lecturer in the Department of Mechanical Engineering at Pekanbaru College of Technology (STTP), Riau, Indonesia. The fields of education that have been taken are a doctoral degree from the Department of Environmental Engineering at the University of Riau in 2023. Became a lecturer with courses in physics, machine kinematics and dynamics, machine maintenance and upkeep, and machine design. Writing in various national and international journals indexed by Scopus, and has several patents and copyrights. He can be contacted at email: joelnaidi@gmail.com.






Nidya Chitranningrum    is a Researcher at the National Research and Innovation Agency of the Republic of Indonesia. She can be contacted at email: nidy001@brin.go.id.



Ahmad Fudholi    is a lecturer at SERI, Universiti Kebangsaan Malaysia, and a Researcher at the National Research and Innovation Agency of the Republic of Indonesia. The fields of education that have been taken are a Ph.D. in Renewable Energy, Solar Energy Research Institute (SERI), UKM, Malaysia, 2012. He can be contacted at email: ahmad.fudholi@brin.go.id.



Rika Taslim    is a Lecturer in the Industrial Engineering Department at the Faculty of Science and Technology, Sultan Syarif Kasim State Islamic University of Riau since January 2014. She is an active Researcher and is trusted as a Reviewer in several reputable international journals. The fields of education that have been taken are S-1 Physics from Riau University in 2001, S-2 and S-3 at University Tenaga Nasional, Malaysia in 2009 and 2013. She can be contacted at email: rikataslim@uin-suska.ac.id.